

Upper mantle SH- and P-velocity structures and compositional models beneath southern Africa

Yi Wang^{*}, Lianxing Wen, Donald Weidner

Department of Geosciences, State University of New York at Stony Brook, United States

Received 13 July 2007; received in revised form 2 December 2007; accepted 9 December 2007

Available online 23 December 2007

Editor: G.D. Price

Abstract

We constrain SH and P wave velocity structures in the upper mantle beneath southern Africa, using triplicated phases recorded in the epicentral distance range of 11°–28° for one shallow event. We then explore thermal and compositional models appropriate for explaining the inferred seismic structures in the region. Both SH and P wave data suggest presence of a low velocity zone with velocity reductions of at least –5% for S waves and –2% for P waves beneath a 150 km thick high-velocity lithospheric lid. Seismic observations also suggest that the P/S ratio is larger (1.88) in the transition zone than in the lithospheric lid (1.70). The inferred P wave velocity jump across the 660-km discontinuity is small (<4%), while the inferred SH wave velocity jump across the discontinuity is comparable to that in the Preliminary Reference Earth Model. The low velocity zone can be explained by a high temperature gradient of 6 °C/km or presence of partial melt. Partial melt would require presence of water or other volatile elements in the depth range of the low velocity zone to lower the mantle solidus. The different P/S velocity ratios between the lithospheric lid and the transition zone can be explained by a difference in aluminum content of mantle composition, with values of 1% in the lithospheric lid and 4% in the transition zone, respectively. The inferred P and SH velocity jumps suggest a bulk sound velocity decrease of 3.4% across the 660-km discontinuity. Such a large decrease of bulk sound velocity is possible only if the bulk modulus of perovskite is similar to those of ringwoodite and garnet, a result remained to be confirmed by experimental or theoretical studies. The presence of the low velocity zone with large velocity reductions beneath southern Africa suggests existence of a low-density anomaly beneath the lithospheric lid, which may provide an explanation to the observed localized uplift in the “African Superswell”.

© 2007 Elsevier B.V. All rights reserved.

Keywords: southern Africa; upper mantle; velocity structures; thermal and compositional model; low velocity zone; P/S velocity ratio; African superswell

1. Introduction

Constraining seismic velocity structure and mantle composition is important in understanding mantle dynamics. When mantle composition is known, mantle density anomalies can be derived from seismic velocity anomalies in the Earth’s mantle. Different mantle compositions and temperatures result in different seismic structures in the upper mantle, and can be directly tested by seismic data. Joint modeling of seismic and

mineral physics data can help us investigate mantle velocity structures and thermal and compositional models.

Southern Africa is a particularly interesting region for studying mantle composition and dynamics. The upper mantle structure beneath southern Africa provides an opportunity to study the depth extent and composition of the cratonic root. The southern African plateau is elevated by more than 1 km above the sea level and the surrounding oceans have a residual bathymetry in excess of 500 m (Nyblade and Robinson, 1994). These elevated regions are termed the “African Superswell” by Nyblade and Robinson (1994). The geoid also exhibits a positive anomaly, but the geoid anomaly is manifested in a broader region in Africa. The sources for the anomalously high

^{*} Corresponding author. Tel.: +1 621 632 1790.

E-mail address: yiwang1@ic.sunysb.edu (Y. Wang).

elevation in the “African Superswell” and the relatively larger scale gravity anomaly in the region are still under debate. While Nyblade and Robinson (1994) suggested that the “African Superswell” may be caused by a thermal anomaly in the lithosphere, Lithgow-Bertelloni and Silver (1998) argued that the superswell can be explained by some density anomaly in the low mantle. The detailed upper mantle velocity structures beneath southern Africa are needed to evaluate these possible proposals for the origin of the “African Superswell”.

In this study, we use joint modeling of seismic and mineral physics data, an approach similar to what we adopted in our previous study of the 660-km discontinuity beneath South America and northeast Asia (Wang et al., 2006), to constrain the seismic P and SH velocity structures and thermal and compositional models in the upper mantle beneath southern Africa. We adopt waveform modeling to constrain the seismic structure. Synthetic waveforms are calculated by a reflectivity program (Zhu and Rivera, 2002). We also explore mantle mineralogical models that are associated with the inferred mantle thermal and compositional models. We discuss seismic data in Section 2, shear and compressional wave velocity structures beneath southern Africa in Sections 3 and 4, thermal, compositional and mineralogical models in Section 5, effects of lateral heterogeneity and attenuation, and comparisons with seismic results from previous studies on southern Africa and the

Canadian Shield in Section 6, and implications for the origin of the “African Superswell” in Section 7.

2. Seismic data

The sampling region of the seismic data is the upper mantle beneath southern Africa (Fig. 1). The P and SH velocity structures of the upper mantle in this region are constrained using the triplicated phases recorded by the Kaapvaal Seismic Array in the epicentral distance range of 11° – 28° for a shallow event occurring in southern Africa. The seismic data of the event have a high signal to noise ratio and are selected from the earthquakes occurring in Africa during the lifetime of the Kaapvaal Array. The source mechanism of this event is 315° for strike, 36° for dip and -133° for slip. The dense coverage of the Kaapvaal Array provides good sampling coverage for the entire depth range in the upper mantle. Our seismic approach is similar to those seismic studies using triplicated phases in the upper mantle distance ranges (e.g., Helmberger and Wiggins, 1971; Burdick and Helmberger, 1978; Given and Helmberger, 1980; Walck, 1984; Grand and Helmberger, 1984a,b; LeFevre and Helmberger, 1989; Cummins et al., 1992; Neele, 1996; Brudzinski and Chen, 1997; Melbourne and Helmberger, 1998; Zhao et al., 1999; Brudzinski and Chen, 2000; Brudzinski and Chen, 2003; Chen and Brudzinski, 2003; Song et al., 2003).

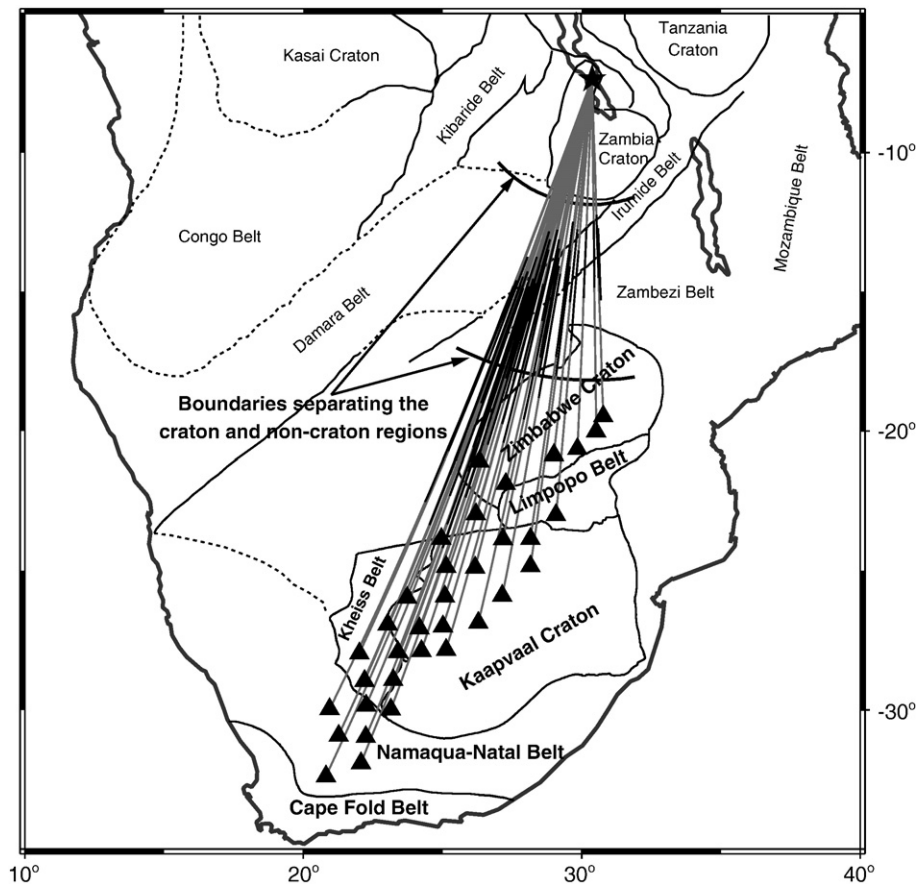


Fig. 1. Map showing great circle paths from seismic event (star) to stations (triangles), with the black segments indicating the portions that the BC branch (defined in Fig. 2) travels below the lithospheric lid, as well as the geologic provinces in southern Africa. The original time of the earthquake is 1997/09/21/18:16:27 and the event depth is 30 km. Two heavy lines represent the boundaries of the finite-difference models in the calculations in Fig. 9.

Several seismic phases can be used to constrain the velocity structures in the upper mantle: the direct phase traveling in the lithospheric lid (AB branch), the reflection off the 410-km discontinuity (BC branch), the wave traveling in the transition zone (CD branch), the reflection off the 660-km discontinuity (DE branch), the wave traveling below the 660-km discontinuity (EF branch) and the wave traveling in the low velocity zone (CG branch) (Fig. 2). The absolute travel time of the AB branch is sensitive to the seismic velocity in the lithospheric lid. The amplitude change of the AB phase with distance is sensitive to presence or absence of a low velocity zone below the lithospheric lid and the onset depth of the low velocity zone. The presence of a low velocity zone would create a shadow zone for the AB branch and generate weak direct arrivals. The onset distance of the observed weakened direct arrivals is controlled by the onset depth of the low velocity zone. The travel time differences between the AB and BC branches and between the AB and CD branches are sensitive to the velocity reduction in the low velocity zone and the depth of the 410-km discontinuity. The travel time difference between the CD and DE branches is sensitive to the depth of the 660-km discontinuity and the velocity structure above the 660-km discontinuity. The travel time difference between the CD and

EF branches is sensitive to the seismic velocity in the transition zone, the velocity jump across the 660-km discontinuity and the depth of the 660-km discontinuity. In the SH data, three phases, AB, CD and EF, can be recognized; while in the P data, only the AB and CD branches can be recognized. The triplications in the upper mantle occur in an epicentral distance range of 11° – 28° , so the data in this epicentral distance range is used. Seismic data are bandpass filtered in a frequency range of 0.05–1 Hz.

3. Upper mantle shear velocity structure beneath southern Africa

Tangential displacements recorded in the Kaapvaal Array for the event constitute a good record section sampling the seismic shear velocity structure in the upper mantle beneath southern Africa (black traces, Figs. 3a, b, S1a and S1b). The event exhibits a simple source time function and three branches of triplications are clearly identifiable in the data. The AB branch turns about 125 km deep in the upper mantle at an epicentral distance of 11° , starts to appear weak at a distance of about 20° and becomes indiscernible at larger distances. The EF phase crosses over the CD phase at about 23.5° and samples a depth of 750 km at 27° (Figs. 3a, b, S1a and S1b).

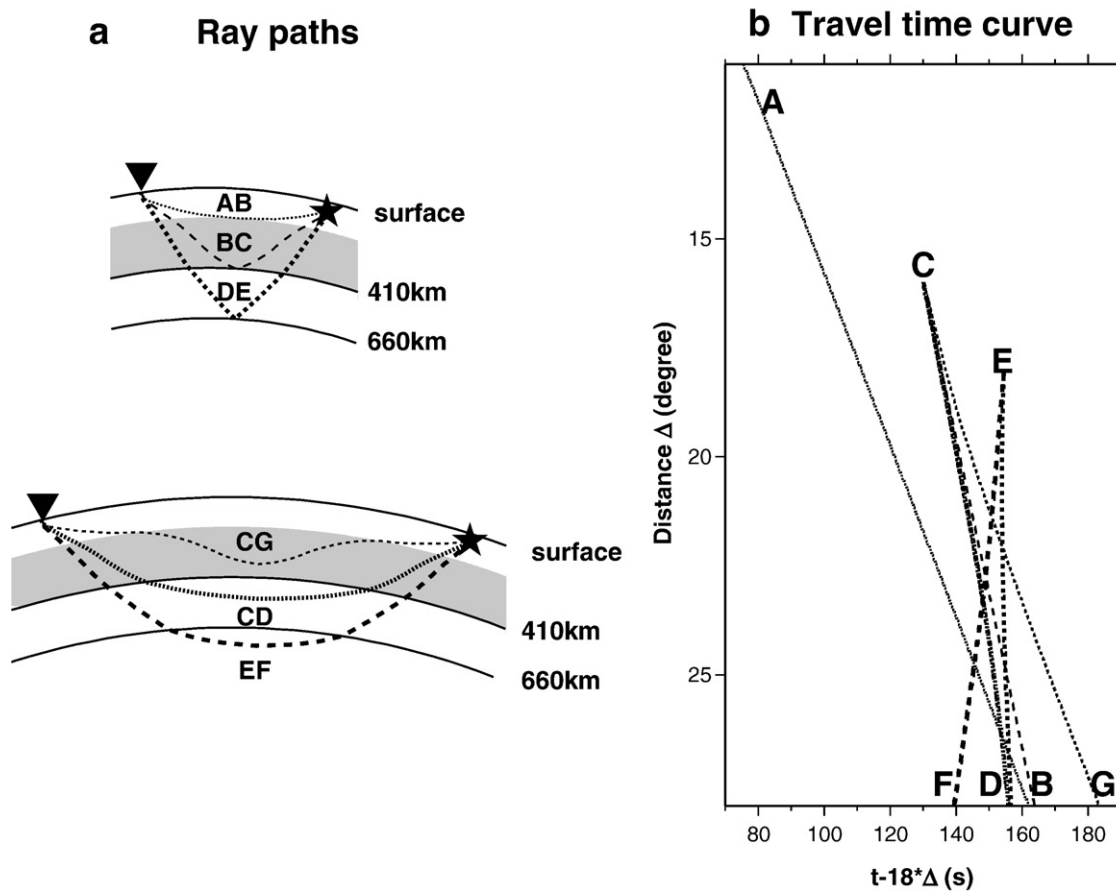


Fig. 2. (a) Ray paths (upper for an epicentral distance of 14° ; lower for an epicentral distance of 25°) and (b) travel time curves of the triplications in the upper mantle for a source depth of 30 km. The shaded regions in (a) represent the low velocity zone. AB branch is the direct wave propagating above the low velocity zone; BC is the reflection off the 410-km discontinuity; CG is the wave traveling in the low velocity zone; CD is the wave traveling in the transition zone; DE is the reflection off the 660-km discontinuity; and EF is the wave traveling below the 660-km discontinuity.

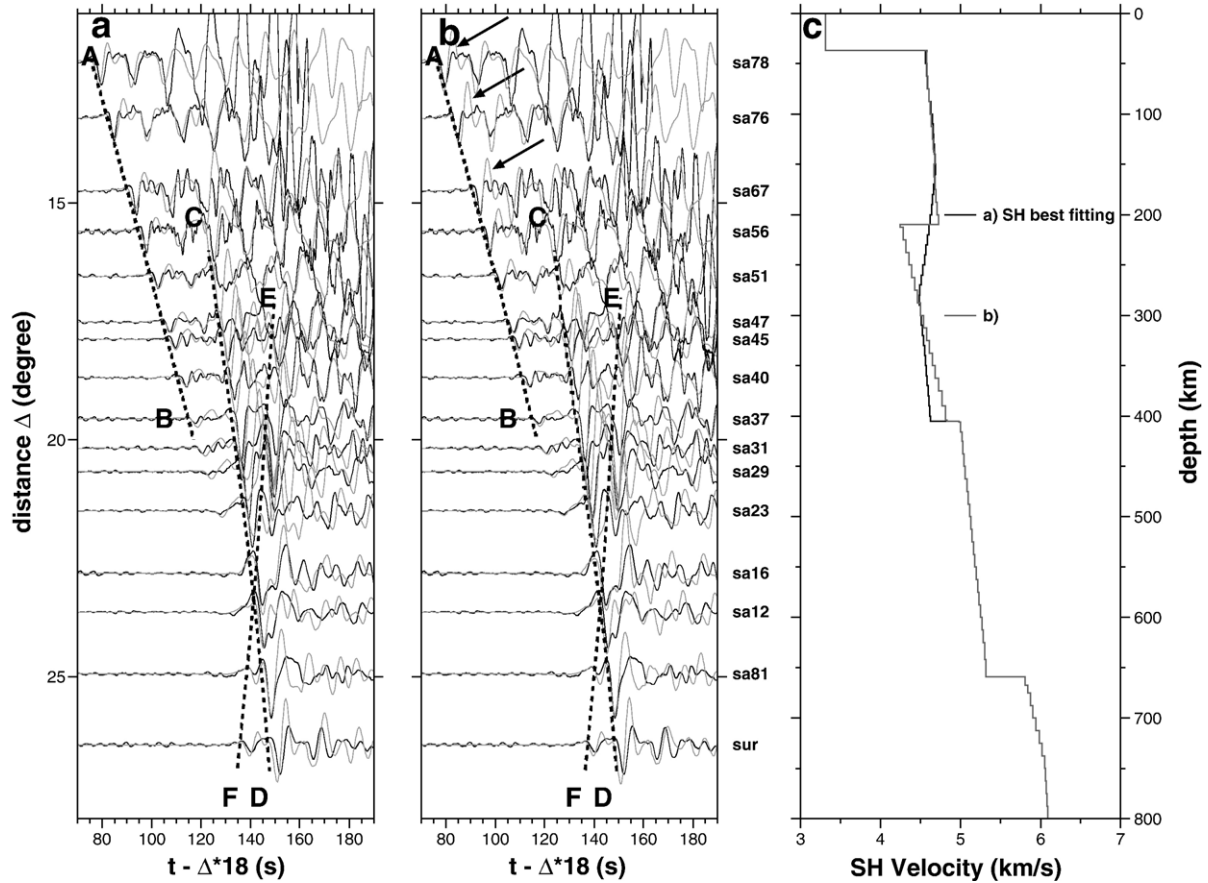


Fig. 3. Comparisons of observed tangential displacements for the seismic waves sampling the upper mantle beneath southern Africa (black traces) and synthetic waveforms (gray traces) calculated using (a) the best fitting model, with a low velocity zone in a depth range of 150 km to 405 km, and (b) a model with a first order discontinuity at the top of the low velocity zone, along with predicted travel time curves of the three branches of the seismic phases (dashed lines). The predicted travel times of different branches of the seismic phases are also labeled. Models are shown in (c) and labeled accordingly with the synthetics panels.

A low velocity zone beneath the high-velocity lid is needed to explain the amplitude decrease of the AB branch with increasing epicentral distance and its disappearance at the distances larger than 20°. In the synthetics based on a model without a low velocity zone, the AB branch extends to an epicentral distance larger than 24°, while the AB branch disappears around 20° in the seismic data (Fig. 4a). The termination distance of the AB branch is sensitive to the onset depth of the low velocity zone. A shallower onset depth of the low velocity zone would make the AB branch disappear at a smaller distance. The amplitude decrease of AB branch, however, does not permit the detailed feature of the low velocity zone to be resolved. The synthetics (gray traces) based on a model with a gradually changing low velocity zone or a model with a first order discontinuity on the top of the low velocity zone would also fit the amplitude decrease of the AB branch and the travel time difference between the AB and CD branches (Figs. 3a, b, S1a and S1b). However, for the model with a first order discontinuity on the top of the low velocity zone, strong reflections off the first order discontinuity (the strong up-swung immediately following the AB branch, pointed by arrows in Figs. 3b and S1) can be clearly recognized in the synthetics, while such strong pulses are not present in the seismic data. Thus, the model with a gradually changing low velocity zone is favored

by the seismic data. The top of the low velocity zone is 150 km deep and the shear velocity reduction is –8.5% (model a, Figs. 3c and S1c).

In explaining the seismic data, however, there is a trade-off between the shear velocity reduction in the low velocity zone and the depth of the 410-km discontinuity. For example, the synthetics calculated based on a model with a 20 km deeper 410-km discontinuity and a smaller velocity reduction in the low velocity zone could fit the seismic data equally well (Fig. 4b). Despite the trade-offs, synthetic tests indicate that a low velocity zone with a minimum velocity reduction of –5% (which would be associated with a 20 km deeper 410-km discontinuity) is required to explain the seismic data.

The absolute S wave velocities and the velocity gradient in the transition zone (0.0013 (km/s)/km) are well constrained by the absolute travel time and the move-out of the CD branch. A larger velocity would make the CD branch arrive earlier, and a larger velocity gradient would cause a larger move-out of the CD branch.

The S wave velocity jump across the 660-km discontinuity (0.5 km/s) is also well constrained by the travel time difference between the CD and EF branches. A larger velocity jump would make the CD branch arrive relatively later or the EF branch

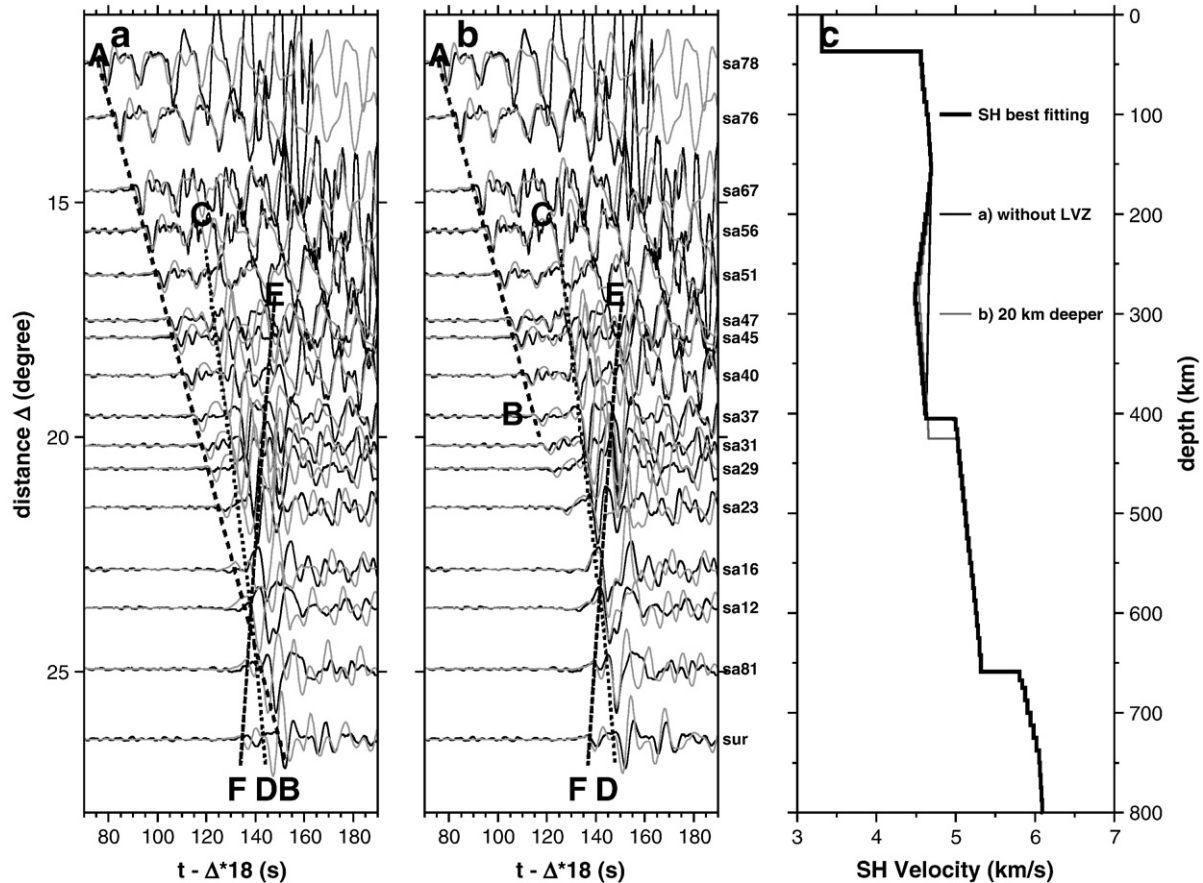


Fig. 4. Comparisons of observed tangential displacements (black traces) and synthetic waveforms (gray traces) calculated using models perturbed from the S wave best fitting model: (a) without a low velocity zone and (b) with a 20 km deeper 410-km discontinuity and a smaller velocity reduction in the low velocity zone, along with predicted travel time curves of the three branches of the seismic phases (dashed lines). Models are shown in (c) and labeled accordingly with the synthetics panels.

relatively earlier, i.e., a larger travel time difference between the CD and EF branches. A smaller velocity jump would do the opposite.

4. Upper mantle compressional velocity structure beneath southern Africa

Only two branches of triplications (the AB and CD branches) are clearly identifiable in the observed vertical displacements (Figs. 5a, b, S2a and S2b). The AB branch turns about 140 km deep in the upper mantle at an epicentral distance of 11° . The CD phase samples the transition zone to a depth of 660 km at 27° . The AB branch can be clearly observed in the data until at a distance of about 17° and becomes indiscernible at larger distances (Figs. 5a, b, S2a and S2b).

A low velocity zone for the P waves is also required to satisfy the travel time difference between the AB and CD branches. In explaining the P wave data, the P velocity in the depth range between 150 km and the 410-km discontinuity trades off with the assumed depth of the 410-km discontinuity. A model with a deeper 410-km discontinuity would require a smaller velocity reduction in the depth range between 150 km and the 410-km discontinuity. A low velocity zone would not be required for the P wave data if the 410-km discontinuity is placed 30 km deeper (Fig. 6a). However, a 30 km deeper 410-km discontinuity

would no longer fit the SH data (Fig. 6b), because the small shear velocity reduction required for a 30 km deeper discontinuity would generate a larger termination distance of the AB phase in SH synthetics than in the data. Thus, a low velocity zone above the transition zone is also required for the P data, and the minimum reduction of P velocity in the low velocity zone is -2% , associated with a 20 km deeper 410-km discontinuity.

The P wave data, however, cannot resolve detailed feature of the low-velocity zone and the inferred P velocity reduction in the low velocity zone would also depend on the assumed feature of the low velocity zone. The synthetics (gray traces) calculated based on a model with a gradually changing low velocity zone or a model with a first order discontinuity on the top of the low velocity zone would fit the seismic data equally well (Figs. 5a, b, S2a and S2b). Since the low velocity zone with a first order discontinuity cannot explain the tangential seismic data, we adopt a P velocity model with a gradually changing low velocity zone. In this model, the top of the low velocity zone is 150 km deep and the velocity reduction is -2% (model a, Figs. 5c and S2c).

The P and SH data also indicate different P to S velocity ratios in the lithospheric lid and in the transition zone. Such feature is well resolved. A uniform P/S velocity ratio in the upper mantle cannot explain the seismic data in the whole

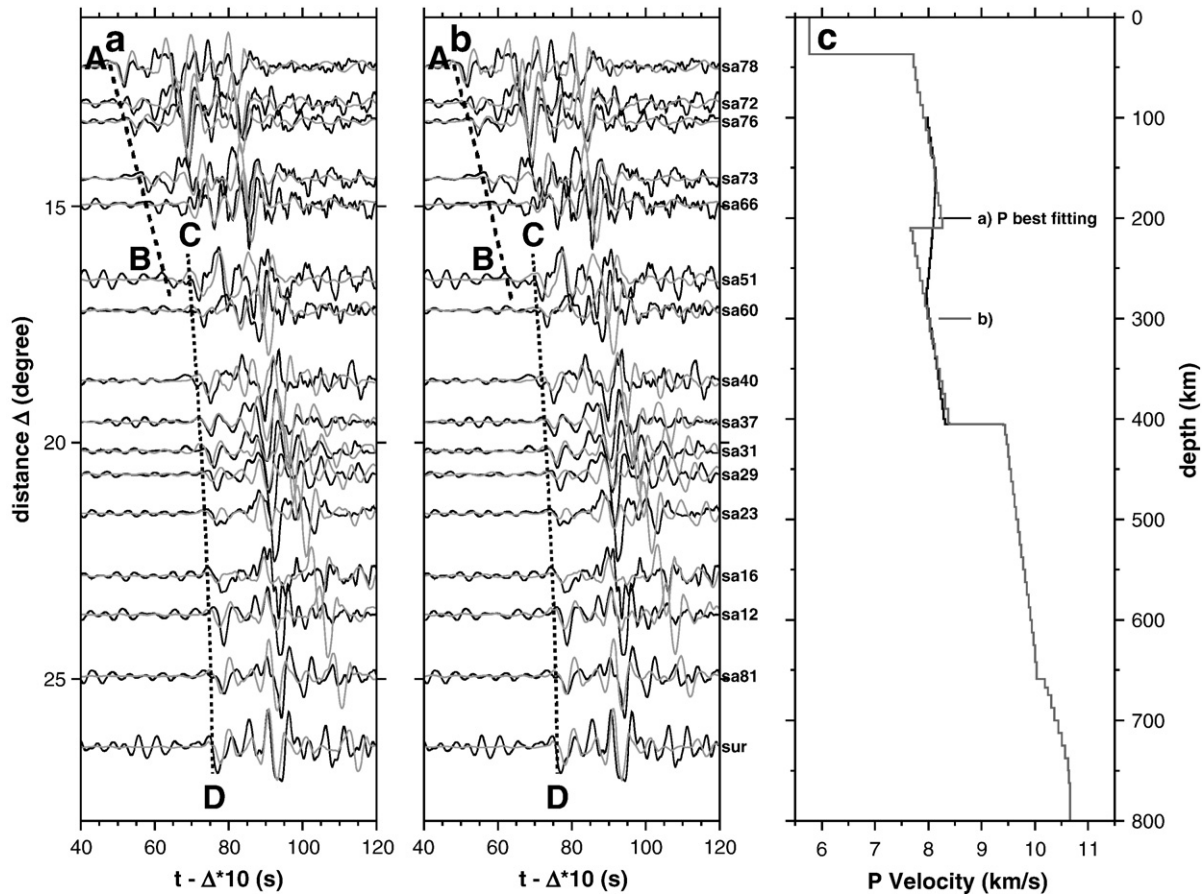


Fig. 5. Comparisons of observed vertical displacements for the seismic waves sampling the upper mantle beneath southern Africa (black traces) and synthetic waveforms (gray traces) calculated using (a) the best fitting model, with a low velocity zone in a depth range of 150 km to 405 km, and (b) a model with a first order discontinuity at the top of low velocity zone, along with predicted travel time curves of the two branches of the seismic phases (dashed lines). Models are shown in (c) and labeled accordingly with the synthetics panels.

distance range. For example, a P velocity model uniformly scaled from the best-fitting S velocity model to fit the arrival times of the AB phase would predict a CD branch much later than that in the seismic data (Fig. 7a).

The triplication associated with the 660-km discontinuity (the waves reflected off and traveling below the 660-km discontinuity), while it is clear in the SH wave data, cannot be recognized in the P wave data. This suggests a small P velocity jump less than 4% across the 660-km discontinuity. A larger P velocity contrast across the discontinuity would predict strong triplication phases of the 660-km discontinuity that are not observed in the data (see Fig. 7b for an example for the synthetics predicted by a model with a velocity jump larger than 4% across the 660-km discontinuity). The large SH velocity jump and the small P velocity jump suggest a bulk sound velocity decrease across the 660-km discontinuity.

5. Thermal, compositional and mineralogical models of the upper mantle beneath southern Africa

5.1. Procedures of thermal and compositional modeling

In this section, we infer mantle thermal and compositional models beneath southern Africa through quantitative compar-

isons between the seismic models obtained from modeling the seismic data and the velocity structures predicted based on various thermal and compositional models. We also explore the mineralogical models associated with the various mantle temperature and composition.

Mantle composition consists of two major components: an olivine-normative ($(\text{Mg,Fe})_2\text{SiO}_4$) component and a pyroxene-normative ($(\text{Mg, Fe})_2\text{SiO}_3$) component. At a pressure of approximately 14 GPa, corresponding to the depth of the 410-km discontinuity, olivine (α -phase) transforms to wadsleyite (β -phase), and pyroxene transforms to garnet, with an increase in seismic velocities and density. At a depth of about 520 km, wadsleyite transforms to ringwoodite (γ -phase). Near the 660-km discontinuity, garnet transforms to perovskite and ringwoodite transforms to perovskite plus magnesiowüstite. At low mantle temperature or/and low Al content, garnet could transform to ilmenite first in the bottom of the transition zone before it starts to transform to perovskite across the 660-km discontinuity. Depending on mantle composition (mostly Al content), the garnet transformation to perovskite could persist to 100 km below the 660-km discontinuity (Wang et al., 2006).

In mineral physics modeling, seismic velocities in the upper mantle are calculated following the procedures outlined in (Weidner and Wang, 1998) and (Wang et al., 2006). We use

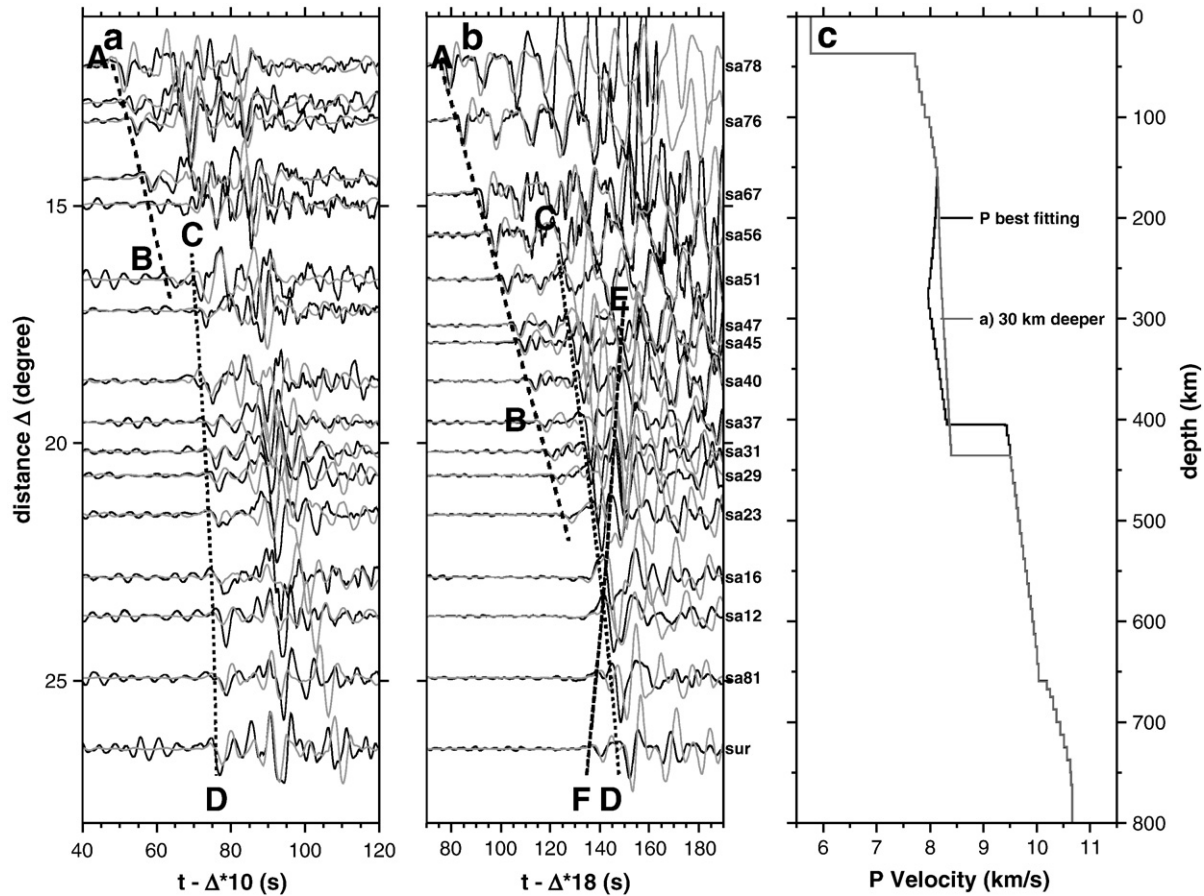


Fig. 6. (a) Comparisons of observed vertical displacements (black traces) and synthetic waveforms (gray traces) calculated using models perturbed from the P wave best fitting model, without a low velocity zone and with a 30 km deeper 410-km discontinuity and (b) comparisons of observed tangential displacements (black traces) and synthetic waveforms (gray traces) calculated using models perturbed from the S wave best fitting model, with a 30 km deeper 410-km discontinuity and a smaller velocity reduction in the low velocity zone, along with predicted travel time curves of the seismic phases (dashed lines). Model (a) and the best fitting P model are shown in (c).

phase equilibria data to define the stable assemblages at relevant pressures and temperatures, and cation distribution data to define the chemical composition of each phase. This information, along with our current estimates of physical properties of these phases, provides a mineralogical model with volume fractions of each phase along with the aggregate velocities and density. In this calculation, we use the phase diagram of CaO–MgO–Al₂O₃–SiO₂ (CMAS) system reported by Gasparik (1996) as a template for defining the evolution of the system through the upper mantle phase transformations. Al contents in spinel and ilmenite are assumed to be negligible in these systems (Gasparik, 1990).

Our approaches are similar to those of a recent study by Stixrude and Lithgow-Bertelloni (2005), but with some differences. In our mineral physical modeling, we take the phase transformations as inputs based on the phase diagram of CaO–MgO–Al₂O₃–SiO₂ (CMAS) system reported by Gasparik (1996), while Stixrude and Lithgow-Bertelloni (2005) calculated the phase transformations based on thermodynamic models. Stixrude and Lithgow-Bertelloni (2005) used the pyrolite bulk composition, while we allow the Al and Fe contents of the mantle composition to vary in matching the

seismic P and S velocities. We have ignored anorthite and the high-pressure polymorph of Mg-rich pyroxene of C2/c symmetry in our system, which were considered in the Stixrude and Lithgow–Bertelloni’s study. The absence of anorthite and the high-pressure polymorph of Mg-rich pyroxene should not be important. Anorthite exists in depths smaller than 100 km, while the focused depths of modeling in the present study are from 100 to 800 km. Because the high-pressure polymorph of Mg-rich pyroxene is absent in our modeling, we have ignored a possible second-order 300-km discontinuity in our predictions.

5.2. Low velocity zone

The low velocity zone beneath the lithospheric lid can be explained by a high temperature gradient or partial melt. The availability of both P and S velocity profiles would allow us to distinguish these two possibilities. Temperature would affect both bulk and shear moduli of the minerals, while partial melt would only mostly affect shear modulus. The velocity reductions in the low velocity zone in our best fitting model would suggest decreases of both shear and bulk moduli, so a high temperature gradient is a more likely explanation. A

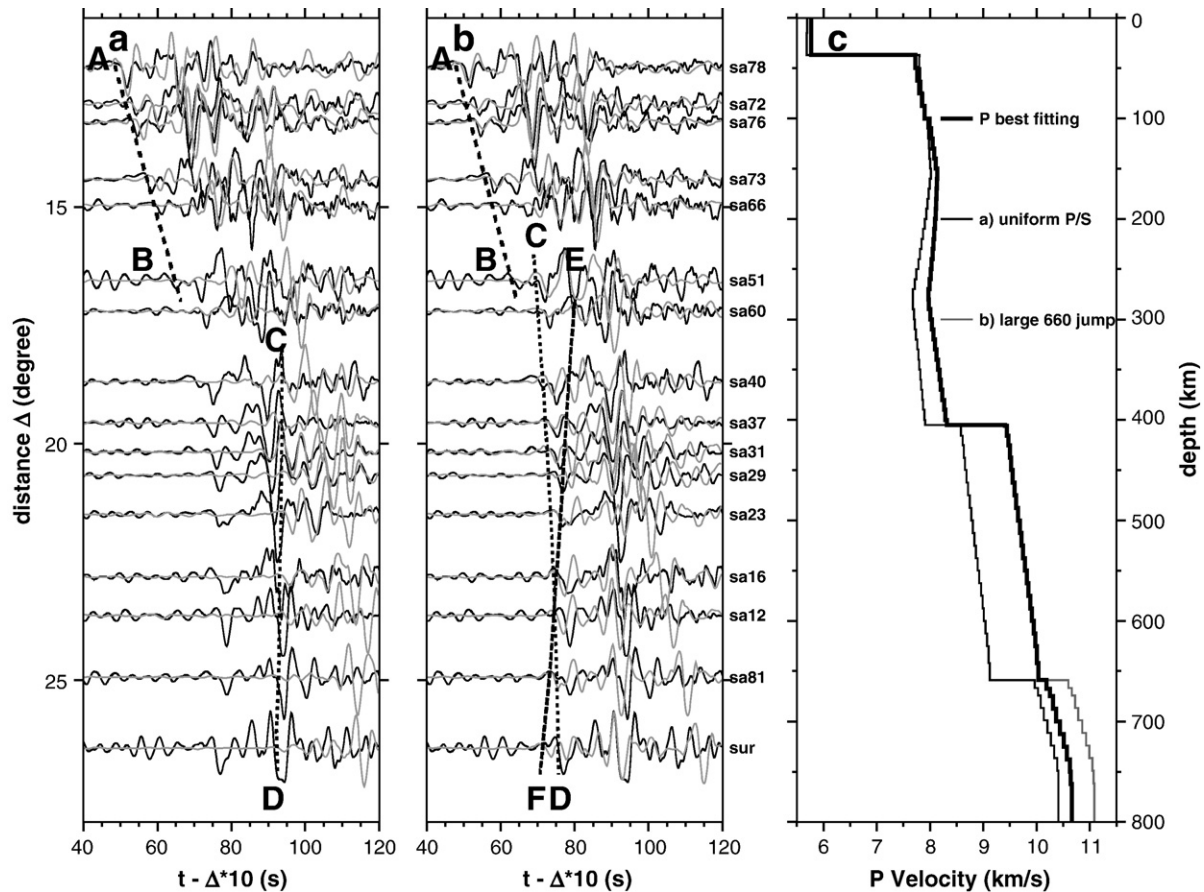


Fig. 7. Comparisons of observed vertical displacements (black traces) and synthetic waveforms (gray traces) calculated using (a) a model converted from the S wave best fitting model with a uniform P to S ratio and (b) a model perturbed from the P wave best fitting model with a larger velocity jump across the 660-km discontinuity, along with predicted travel time curves of the two branches of the seismic phases (dashed lines). Models are shown in (c) and labeled accordingly with the synthetics panels.

temperature gradient of about 6 °C/km in the depth range of 150–275 km (Fig. 8d) is needed to satisfy the minimal shear velocity reduction of -5% inferred for the low velocity zone beneath southern Africa. Such a temperature gradient would indicate that the mantle density in the low velocity zone is about 4% smaller than the density in lithospheric lid. If partial melt is involved, presence of water or other volatile elements would be required in the depth range of the low velocity zone to suppress the solidus, as the solidus of the dry peridotite (Zhang, 1994) would be higher than the inferred temperature, even with a temperature gradient of 6 °C/km (Fig. 8d).

5.3. Different P/S ratios in the lithospheric lid and the transition zone

The different P to S velocity ratios between the lithospheric lid and the transition zone can be explained by a difference in aluminum content of the mantle composition in the two depth regions. A higher aluminum content would result in more garnet and less clinopyroxene and orthopyroxene (Fig. 8f). Because the bulk modulus of garnet is much larger than those of clinopyroxene and orthopyroxene, and the shear modulus of garnet is only slightly larger than those of clinopyroxene and orthopyroxene, a higher aluminum content would cause a higher P wave velocity,

but a similar S wave velocity and, thus, a higher P to S velocity ratio. In the lithospheric lid, a compositional model with an aluminum content of 1% can explain the absolute seismic velocities and the P to S velocity ratio. A lower aluminum content results in more clinopyroxene and orthopyroxene and less garnet (Fig. 8e) and thus a lower P/S velocity ratio (Fig. 8c) in the lithospheric lid. In the transition zone, the higher P to S velocity ratio requires a higher aluminum content of 4%. A higher aluminum content results in more garnet and less clinopyroxene and orthopyroxene in the transition zone, and thus a higher P to S velocity ratio (Fig. 8c). The lower Al content inferred for the lithospheric lid could result from the depletion of the basaltic component of the mantle composition beneath the old continental nuclei, consistent with the tectosphere hypothesis beneath the continental cratons (Jordan, 1978).

5.4. The bulk sound velocity decrease across the 660-km discontinuity

The PREM-like SH velocity jump and a small P velocity jump across the 660-km discontinuity suggest a bulk sound velocity decrease of 3.4% across the 660-km discontinuity. The decrease in bulk sound velocity across the 660-km discontinuity seems to be consistent with the results from the first principle

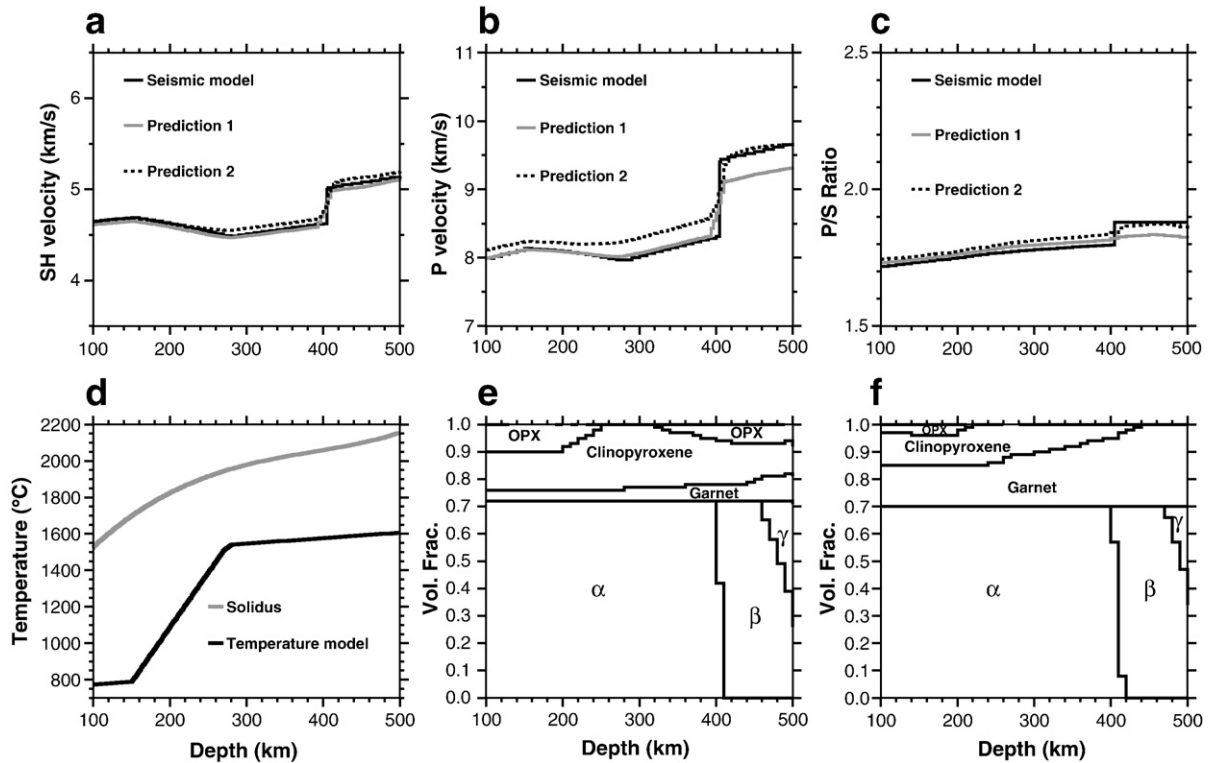


Fig. 8. (a–c) comparisons between seismic velocity models and the predictions based on two mantle compositional models, (a) for S wave velocities, (b) for P wave velocities and (c) for P to S velocity ratios; (d) thermal model and the solidus for the anhydrous peridotite (Jordan, 1978); and (e–f) mineralogical models predicted based on the thermal model in (d) and two mantle compositional models with Al contents of 1% (e) and 4% (f). α denotes olivine; β wadsleyite; γ ringwoodite; and OPX orthopyroxene.

calculation for the ringwoodite (pure Mg_2SiO_4 , without Fe and Al) to perovskite and magnesiowustite phase transformation by Yu et al. (2007), which find a bulk sound velocity decrease of $0.1 \pm 0.48\%$ across the phase transformation boundary. But, the bulk sound velocity reduction is much larger in the seismic results than in the first principle calculations. Based on current estimates of elastic properties of mantle phases, we are not able to predict a bulk sound velocity decrease with a magnitude of 3.4%. Such a large decrease of bulk sound velocity would require the bulk modulus of perovskite to be similar to those of ringwoodite and garnet at the pressure and temperature conditions around the 660-km discontinuity, a result remained to be confirmed by experimental or theoretical studies.

6. Discussions

6.1. Effects of lateral variation of seismic structure on the inference of the low velocity zone

The primary evidence for the existence of a low velocity zone beneath the lithosphere in southern Africa is the decreasing amplitude and eventual disappearance of the AB branch observed at large distances in the SH data (Fig. 3a); and the above inference of the low velocity zone is based on one-dimensional (1D) seismic modeling. However, the Kaapvaal Seismic Array locates across several cratons (the Kaapvaal Craton, the Limpopo Belt, the Zimbabwe Craton, the Kheiss Belt and the Namaqua–Natal Belt) and the epicenter of the

event is in another craton, the Zambia Craton (Fig. 1). Seismic waves sample regions across the Zambia Craton, the non-cratonic regions of the Irumide Belt and the Zambezi Belt, and the cratonic region of the Zimbabwe Craton, the Limpopo Belt and the Kaapvaal Craton (Fig. 1). Lateral variation of velocity exists along the seismic paths and it is important to access the effects of the lateral velocity variation on the amplitude of the AB branch. We use a finite-difference method (Vidale and Helmberger, 1987) and test many two-dimensional (2D) seismic velocity models to study such effects. Based on Li and Burke's three-dimensional (3D) S wave velocity model (Li and Burke, 2006), the lateral variations between the Kaapvaal Craton, the Limpopo Belt, the Zimbabwe Craton, the Kheiss Belt and the Namaqua–Natal Belt are small, so we approximate them as one region with an 1D velocity structure. Based on Priestley et al.'s SV-velocity model in southern Africa (Priestley et al., 2006), at depths of 150 km and 250 km, the Zambia Craton and the Zimbabwe Craton have almost the same velocity, so we also used the 1D cratonic velocity model for the Zambia Craton. We thus test 2D models that comprise of two different 1D SH velocity structures along the paths, representing the velocity structures in and out of the cratons, respectively. We show synthetic examples for models with the boundaries that separate the cratonic and non-cratonic regions shown in Fig. 1. The boundary between the non-craton region and the Zimbabwe Craton in these example models do not exactly coincide with the geological boundary of the Zimbabwe Craton, but finite-difference models with boundaries coinciding with the

northernmost and southernmost the Zimbabwe Craton show similar results discussed below. Synthetics show that models with lateral velocity variation in the lithospheres, but without a low-velocity zone beneath the lithospheric lid, cannot explain the seismic data. Models with the non-cratonic region having same velocity gradient as in the cratonic region, but having smaller absolute velocities, cannot generate the distance dependence of the amplitude of the AB phase as observed in the data (Fig. 9a). Models with a larger velocity gradient in the non-cratonic region could generate a decrease of the amplitude of the AB phase with increasing epicentral distance in the synthetics. But the predicted change is much smaller than the observed and the predicted AB termination distance is much larger than what observed in the data. Even if we adopt a velocity gradient of 0.004712 km/s/km in the non-cratonic region, a gradient that would generate much larger travel times and a very different move-out of the AB phases than observed (Fig. 9c), the synthetics based on this model cannot fit the distance dependence of the AB amplitude and the AB termination distance observed in the seismic SH data (Fig. 9b). We thus conclude that the velocity variations between the cratonic and non-cratonic regions cannot explain the observed distance dependence of amplitude and the eventual termination of the AB phase at large distances in the seismic

data. A low velocity zone beneath the lithospheric lid is required to explain these waveform characteristics.

6.2. Attenuation effect

We did not include attenuation effect in our synthetic calculations. A very high attenuation channel in the depths of the low velocity zone would generate an amplitude decrease of the AB phase at large epicentral distances, similar to the effect of a low velocity zone. However, synthetics tests indicate that such a high attenuation channel would also generate small amplitudes of the CD and EF phases and cannot explain the observed amplitude ratios between the CD and AB branches in the epicentral distance range between 15° and 22°, and the observed amplitudes of the EF branch at large distances. Thus, the seismic data cannot be explained by attenuation effect; a low velocity zone is required. Synthetics tests further indicate that attenuation affects little the inference of the different P/S ratios between the lithospheric lid and the transition zone.

6.3. Comparisons with other models in southern Africa

Although different types of the seismic data were used, our best-fitting S velocity model is similar to the results of most of the

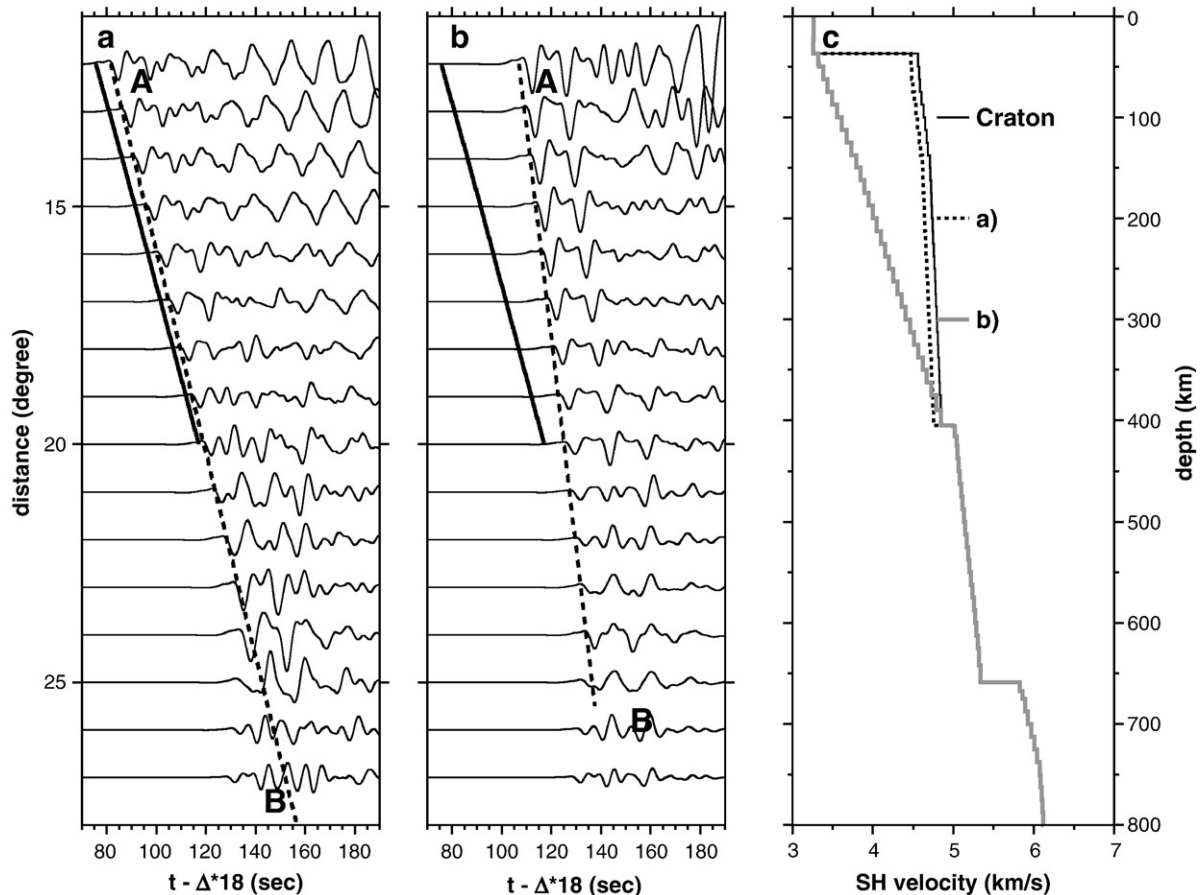


Fig. 9. SH finite difference synthetic waveforms calculated based on two models with same SH velocity structure in the cratonic regions and two different SH velocity structures in the non-cratonic region having a) a smaller absolute velocity and b) a large velocity gradient in the lithospheric lid, along with predicted (dashed lines) and observed (solid lines) travel time curves of the AB branch. Velocity models are shown in c) and labeled accordingly with the synthetics panels.

previous surface wave studies. Earlier surface wave studies (Bloch et al., 1969; Qiu et al., 1996) showed a thinner lithospheric lid and a stronger S wave low velocity zone than our best-fitting model beneath southern Africa. Later studies (Priestly, 1999; Priestly et al., 2006; Li and Burke, 2006), however, indicated a model similar to our best-fitting SH velocity model, in having similar thickness, and onset depth and magnitude of S wave velocity reduction of the low velocity zone. Freybourger et al. (2001) found that the upper mantle beneath the Kaapvaal Craton is anisotropic from beneath the Moho to about 100 km depth, using the fundamental modes of the Love and Rayleigh wave phase velocities, but most of other studies did not find any evidence of anisotropy in this region (Qiu et al., 1996; Priestly, 1999). The fact that a low velocity zone was also present in the Rayleigh wave studies (Priestly et al., 2006; Li and Burke, 2006) suggests that the presence of the low velocity zone beneath the lithospheric lid is not the result of seismic anisotropy. The seismic data we used permit us to resolve several additional important features of the seismic structure that the surface wave data did not, including the velocity gradients in the lithospheric lid and the transition zone, velocity structure below 400 km, and both P and S velocity structures.

Receiver function studies (Vinnik et al., 1996; Gao et al., 2002; Stankiewicz et al., 2002) indicated that the thickness of the transition zone is similar to the global average and suggested that the transition zone beneath southern Africa is not anomalously warm. Some receiver function study (Gao et al.,

2002) did not find evidence for a low velocity zone, while others (Vinnik et al., 1996; Stankiewicz et al., 2002) found a weaker and deeper (>300 km) S wave low velocity zone than that in our best-fitting SH velocity model. In those receiver function studies, the thickness of the transition zone and the depths of the discontinuities are inferred on the basis of the IASP91 (Kennett, 1991) model, which is different from our best-fitting southern Africa velocity model (Fig. 10). Thus, the inferred transition zone thickness and discontinuity depths could be different between different studies.

There are also many studies using triplication data in southern Africa (Zhao et al., 1999; Simon et al., 2002; Wright et al., 2002; Simon et al., 2003; Wright et al., 2004). Zhao et al. (1999) used both travel time and waveform data to constrain the P and S velocity models in the upper mantle beneath southern Africa. Because of the absence of the P waveform data from the epicentral distances less than 2200 km, they could not constrain the detailed velocity structure in the top 300 km of the mantle. Lack of S data prevented them from constraining detailed S velocity structure in the region. Using travel time and waveform information of the triplication data, Simon et al. (Simon et al., 2002, 2003) and Wright et al. (2002, 2004) inferred an S velocity model that has a lithospheric lid with a smaller thickness and similar velocities as our best-fitting SH velocity model, a low velocity zone with a first order discontinuity and a smaller velocity reduction, and a larger velocity gradient and larger velocities in the transition zone. Their P velocity model has larger velocities in the lithospheric lid and

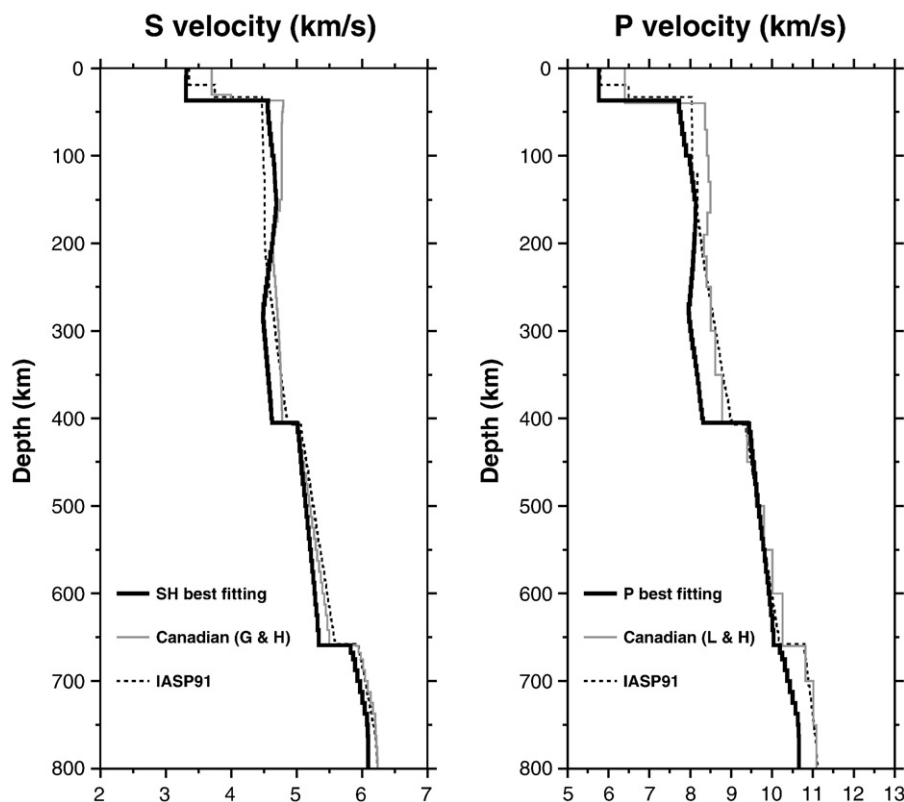


Fig. 10. Comparisons between our best fitting models, two published upper mantle velocity models for the Canadian Shield, Canadian (G & H) (Grand and Helmberger, 1984b) and Canadian (L & H) (LeFevre and Helmberger, 1989), and IASP91: (a) for S velocity and (b) for P velocity.

does not have a low velocity zone in the upper mantle. The sampling region of their seismic data is a broad region of southern Africa, including the Zimbabwe Craton, the Limpopo Belt, the Kaapvaal Craton, the Namaqua–Natal mobile Belt and the Cape Fold Belt, while our sampling region is only the western part of the Zimbabwe Craton and some non-cratonic regions (Fig. 1). The difference in sampling region in their studies may cause those velocity model differences.

6.4. Comparison to velocity models for the Canadian Shield

Our best fitting models exhibit similar characteristics as the P and S velocity model for the Canadian Shield (Grand and Helmberger, 1984b; LeFevre and Helmberger, 1989) in having a high-velocity lithospheric lid overlying a low velocity zone (Fig. 10). However, our best fitting models have lower absolute P and S velocities in the lithospheric lid and a thinner low velocity zone with much larger velocity reductions. The P velocity jump across the 660-km discontinuity beneath the Canadian Shield is larger than that beneath southern Africa. The S wave model for the Canadian Shield was derived using travel times of S and SS phases recorded in the epicentral distance range of 10°–60° (Grand and Helmberger, 1984b) and the P wave model for the Canadian Shield was derived using waveform modeling Pnl, P and PP phases (LeFevre and Helmberger, 1989). The lower S and P velocities in the lithospheric lid in our model suggest a higher mantle temperature or a lower Al content, or both, in the lithospheric lid in southern Africa than that in the Canadian Shield. The thinner low velocity zone suggests that a thinner layer of the high temperature gradient. The P/S velocity ratios in the lithospheric lid and in the transition zone beneath the Canadian Shield can be explained by a uniform Al content of 4%. Since the P and S velocity models for the Canadian Shield were derived in different studies and were constrained by different seismic datasets, it is unclear that a uniform Al content for both the lithospheric lid and the transition zone found for the Canadian Shield is due to the fact that different datasets were used to infer the P and S velocity models and the uncertainties are different for these P and S velocity models, or the Al contents in the lithospheric lids are different between the Canadian Shield and southern Africa.

7. Implications to the origin of the “African Superswell”

The presence of a low velocity zone with large velocity reductions in the upper mantle beneath southern Africa suggests a low-density anomaly in the upper mantle beneath southern Africa. The presence of a low-density anomaly beneath the lithospheric lid is consistent with the observed localized uplift and broad geoid anomalies in the region of the “African Superswell”. The shallow low-density buoyancy generates large uplifts in the region, but little localized geoid anomaly because of the near-perfect compensation of the topography (Wen and Anderson, 1997; Richards and Hager, 1984). In this case, the localized uplift is caused by the low-density anomaly in the low-velocity zone beneath the lithospheric lid, while the geoid

anomaly observed in a broader region of Africa may be attributed to the large-scale density anomalies in the lower mantle (Wang and Wen, 2007). The presence of a high temperature anomaly in the shallow mantle is also consistent with the high heat flow observed on the ocean floor of the “African Superswell” (Nyblade and Robinson, 1994).

8. Conclusions

We study seismic SH and P velocity structures, mineralogical, thermal and compositional models in the upper mantle beneath southern Africa, through joint modeling of seismic and mineral physics data. Our seismic data consist of the tangential and vertical components of triplicated phases recorded in the epicentral distance range of 11°–28° for a shallow event occurring in southern Africa. The data suggest that the lithospheric lid is about 150 km thick, a low velocity zone below the lithospheric lid beneath southern Africa exists for both P and S velocity structures with velocity reductions of at least –5% for S waves and –2% for P waves, the P to S velocity ratio in the transition zone (1.88) is larger than in the lithospheric lid (1.70), and bulk sound velocity decreases about 3.4% across the 660-km discontinuity.

We infer mantle thermal and compositional models in this region through quantitative comparisons between the P and S seismic models obtained from modeling the seismic data and the velocity structures predicted based on various mantle thermal and compositional models. The low velocity zone can be explained by a high temperature gradient of 6 °C/km or presence of partial melt. The presence of partial melt would require presence of water or other volatile elements in depth range of the low velocity zone to lower the solidus. The difference in P to S ratio between the transition zone and the lithospheric lid can be explained by aluminum contents of 4% in the transition zone and 1% in the lithospheric lid. The inferred lower Al content in the lithospheric lid is consistent with the basaltic depletion in the cratonic tectosphere. The inferred large decrease of bulk sound velocity of 3.4% across the 660-km discontinuity would be possible only if the bulk modulus of perovskite is similar to those of ringwoodite and garnet at the pressure and temperature conditions of the 660-km discontinuity, a result remained to be confirmed by experimental or theoretical studies.

The presence of a low velocity zone with large velocity reductions in the upper mantle beneath southern Africa suggests existence of a low-density anomaly with a dense perturbation of –4% beneath the lithospheric lid beneath southern Africa. The existence of such a low-density anomaly could explain the observed localized uplift in the “African Superswell” and is consistent with the observed broad distribution of the geoid anomaly in the region.

Acknowledgements

We thank the principal investigators of the Kaapvaal Seismic Array for their efforts of collecting seismic data, and Sue Webb and Matthew Fouch for the digitized geological boundaries. This project is supported by an NSF CSEDI grant EAR-0439978.

Appendix A. Supplementary data

Supplementary data associated with this article can be found, in the online version, at doi:10.1016/j.epsl.2007.12.010.

References

- Bloch, S., Hales, A.L., Landisman, M., 1969. Velocities in the crust and upper mantle of southern Africa from multi-mode surface wave dispersion. *Bull. Seism. Soc. Am.* 159, 1599–1629.
- Brudzinski, M.R., Chen, W.P., 1997. Variations of P wave speeds in the mantle transition zone beneath the northern Philippine Sea. *J. Geophys. Res.* 102, 11,815–11,827.
- Brudzinski, M.R., Chen, W.P., 2000. Variations in P wave speeds and outboard earthquakes: evidence for a petrologic anomaly in the mantle transition zone. *J. Geophys. Res.* 105, 21,661–21,682.
- Brudzinski, M.R., Chen, W.P., 2003. A petrologic anomaly accompanying outboard earthquakes beneath Fiji–Tonga: Corresponding evidence from broadband P and S waveforms. *J. Geophys. Res.* 108. doi:10.1029/2002JB002012.
- Burdick, L.J., Helmberger, D.V., 1978. The upper mantle P velocity structure of the Western United States. *J. Geophys. Res.* 83, 1699–1712.
- Chen, W.P., Brudzinski, M.R., 2003. Seismic anisotropy in the mantle transition zone beneath Fiji–Tonga. *Geophys. Res. Lett.* 30. doi:10.1029/2002GL016330.
- Cummins, P.R., Kennett, B.L.N., Bowman, J.R., Bostock, M.G., 1992. The 520 km discontinuity? *Bull. Seismol. Soc. Am.* 82, 323–336.
- Freybourger, M., Gaherty, J.B., Jordan, T.H., and the Kaapvaal Seismic Group, 2001. Structure of the Kaapvaal craton from surface waves. *Geophys. Res. Lett.* 28, 2489–2492.
- Gao, S.S., Silver, P.G., Liu, K.H., and the Kaapvaal Seismic Group, 2002. Mantle discontinuities beneath Southern Africa. *Geophys. Res. Lett.* 29. doi:10.1029/2001GL013934.
- Gasparik, T., 1990. Phase relations in the transition zone. *J. Geophys. Res.* 95, 15,751–15,769.
- Gasparik, T., 1996. Melting experiments on the enstatite–diopside join at 70–224 kbar, including the melting of diopside. *Contrib. Mineral. Petrol.* 124, 139–153.
- Given, J.W., Helmberger, D.V., 1980. Upper mantle structure of northwestern Eurasia. *J. Geophys. Res.* 85, 7183–7194.
- Grand, S.P., Helmberger, D.V., 1984a. Upper mantle shear structure beneath the Northwest Atlantic Ocean. *J. Geophys. Res.* 89, 11,465–11,475.
- Grand, S.P., Helmberger, D.V., 1984b. Upper mantle shear structure of North America. *J. Geophys. Res.* 89, 399–438.
- Helmberger, D.V., Wiggins, R.A., 1971. Upper mantle structure of Midwestern United States. *J. Geophys. Res.* 76, 3229–3245.
- Jordan, T.H., 1978. Composition and development of the continental tectosphere. *Nature* 274, 544–548.
- Kennett, B., 1991. Seismic velocity gradients in the upper mantle. *Geophys. Res. Lett.* 18, 115–118.
- LeFevre, L.V., Helmberger, D.V., 1989. Upper mantle P velocity structure of the Canadian Shield. *J. Geophys. Res.* 94, 17,749–17,765.
- Li, A., Burke, L., 2006. Upper Mantle structure of southern Africa from Rayleigh wave tomography. *J. Geophys. Res.* 111. doi:10.1029/2006JB004321.
- Lithgow-Bertelloni, C., Silver, P.G., 1998. Dynamic topography, plate driving forces, and the African superswell. *Nature* 395, 269–273.
- Melbourne, T., Helmberger, D., 1998. Fine structure of the 410-km discontinuity. *J. Geophys. Res.* 103, 10,091–10,102.
- Neele, F., 1996. Sharp 400-km discontinuity from short-period P reflections. *Geophys. Res. Lett.* 23, 419–422.
- Nyblade, A.A., Robinson, S.W., 1994. The African superswell. *Geophys. Res. Lett.* 21, 765–768.
- Priestley, K., McKenzie, D., Debayle, E., 2006. The state of the upper mantle beneath southern Africa. *Tectonophysics* 416, 101–112.
- Priestly, K., 1999. Velocity structure of the continental upper mantle: evidence from southern Africa. *Lithos* 48, 45–56.
- Priestly, K., McKenzie, D., Debayle, E., 2006. The state of the upper mantle beneath southern Africa. *Tectonophysics* 416, 101–112.
- Qiu, X., Priestley, K., McKenzie, D., 1996. Average lithospheric structure of southern Africa. *Geophys. J. Int.* 127, 563–587.
- Richards, M.A., Hager, B.H., 1984. Geoid anomalies in a dynamic Earth. *J. Geophys. Res.* 89, 5987–6002.
- Simon, R.E., Wright, C., Kgaswane, E.M., Kwadiba, M.T.O., 2002. The P wavespeed structure below and around the Kaapvaal craton to depth of 800 km, from traveltimes and waveforms of local and regional earthquakes and mining-induced tremors. *Geophys. J. Int.* 151, 132–145.
- Simon, R.E., Wright, C., Kwadiba, M.T.O., Kgaswane, E.M., 2003. Mantle structure and composition to 800-km depth beneath southern Africa and surrounding oceans from broadband body waves. *Lithos* 71, 353–367.
- Song, T.A., Helmberger, D.V., Grand, S.P., 2003. Low-velocity zone atop the 410-km seismic discontinuity in the northwestern United States. *Nature* 427, 530–533.
- Stankiewicz, J., Chevrot, S., van der Hilst, R.D., de Wit, M.J., 2002. Crustal thickness, discontinuity depth, and upper mantle structure beneath southern Africa: constraints from body wave conversions. *Phys. Earth Planet. Inter.* 130, 235–251.
- Stixrude, L., Lithgow-Bertelloni, C., 2005. Mineralogy and elasticity of the oceanic upper mantle: Origin of the low-velocity zone. *J. Geophys. Res.* 110, B03204. doi:10.1029/2004JB002965.
- Vidale, J.E., Helmberger, D.V., 1987. Path effects in strong motion seismology. In: Bolt, B.A. (Ed.), *Seismic strong motion synthetics. Comput. techniques*, vol. 4. Academic Press, Orlando, Fla.
- Vinnik, L.P., Green, R.W.E., Nicolaysen, L.O., Kosarev, G.L., Petersen, N.V., 1996. Deep seismic structure of the Kaapvaal craton. *Tectonophysics* 262, 67–75.
- Walck, M.C., 1984. The P-wave upper mantle structure beneath an active spreading center: the Gulf of California. *Geophys. J. R. astr. Soc.* 76, 697–723.
- Wang, Y., Wen, L., 2007. Geometry and P and S velocity structure of the “African Anomaly”. *J. Geophys. Res.* 112. doi:10.1029/2006JB004483.
- Wang, Y., Wen, L., Weidner, D.J., He, Y., 2006. SH velocity and compositional models near the 660-km discontinuity beneath south America and northeast Asia. *J. Geophys. Res.* 111. doi:10.1029/2005JB003849.
- Weidner, D.J., Wang, Y., 1998. Chemical- and Clapeyron-induced buoyancy at the 660 km discontinuity. *J. Geophys. Res.* 103, 7431–7441.
- Wen, L., Anderson, D.L., 1997. Layered Mantle Convection: A Model for Geoid and Topography. *Earth Planet. Sci. Lett.* 146, 367–377.
- Wright, C., Kwadiba, M.T.O., Kgaswane, E.M., Simon, R.E., 2002. The structure of the crust and upper mantle to depth of 320 km beneath the Kaapvaal craton, from P wave arrivals generated by regional earthquakes and mining-induced tremors. *J. Afr. Earth. Sci.* 35, 477–488.
- Wright, C., Kwadiba, M.T.O., Simon, R.E., Kgaswane, E.M., Nguuri, T.K., 2004. Variations in the thickness of the crust of the Kaapvaal craton, and mantle structure below southern Africa. *Earth Planets Space* 56, 125–137.
- Yu, Y.G., Wentzcovitch, R.M., Tsuchiya, T., Umemoto, K., Weidner, D.J., 2007. First principle investigation of the postspinel transition in Mg₂SiO₄. *Geophys. Res. Lett.* 34. doi:10.1029/2007GL029462.
- Zhang, J., 1994. Melting experiments on anhydrous peridotite KLB-1 from 5.0 to 22.5 Gpa. *J. Geophys. Res.* 99, 17,729–17,742.
- Zhao, M.C., Langston, C.A., Nyblade, A.A., Owens, T.J., 1999. Upper mantle velocity structure beneath southern Africa from modeling regional seismic data. *J. Geophys. Res.* 104, 4783–4794.
- Zhu, L.P., Rivera, L.A., 2002. A note on the dynamic and static displacements from a point source in multilayered media. *Geophys. J. Int.* 148, 619–627.